Microstructure characterization and cation distribution of nanocrystalline Sn^{4+} substituted $NiFe_2O_4$

A. ADAM, Z. ALI[*], E. ABDELTWAB, Y. ABBAS[b]
Physics Department, Faculty of Science (Girls Branch), Al-Asher University, Cairo, Egypt
[b]*Physics Department, Faculty of Science, Suez canal University, Ismailia, Egypt*

A series of nanocrystalline Sn^{4+} substituted $NiFe_2O_4$ with general formula $Ni_{1+x}Sn_x Fe_{2-2x}O_4$ (x = 0.0, 0.1, 0.2, 0.3, 0.4, and 0.5) has been prepared by co-precipitation synthetic method. The prepared compounds have been sintered at 1000 °C. The structural and microstructural evolutions of the nanophase have been studied by X-ray powder diffraction and the Rietveld method. The X-ray diffraction patterns showed that all the samples have cubic structure with the space group Fd-3m. The structural parameters were obtained by X-ray diffraction (XRD) spectra fitting refinement using the Rietveld method. Microstructure characterization by TEM corroborates the findings of X-ray analysis.

1. Introduction

Spinels of general formula AB_2O_4 are known to be technologically important materials because of their tailor able properties to meet stringent requirements in various applications [1, 2]. Especially ferrites belonging to this class of materials are gaining prominence owing to their efficacious properties such as high thermodynamic stability, high electrical conductivity, and high corrosion resistance, making them suitable in metallurgical field and other high temperature areas.

Earlier studies have been made to evaluate structural, electrical, and morphological features of $NiFe_2O_4$ synthesized by various methods [3, 4]. It has been reported that the substitution on A-site or B-site of this compound improves its overall properties. The substitution has been tried to synthesize different compositions of ferrites such as Ni–Zn, Ni–Pb, Ni–Cu, Ni–Al, Ni–Mn, Ni–Gd, Ni–Mg, and Ni–Co [5-12]. The magnetic studies on Sn substituted nickel ferrite have been reported in detail [13]. The conventional way of preparing the ferrite is by solid-state reaction, which involves the mixing of oxides with intermittent grinding followed by high temperature sintering between 1300 and 1700 °C. Though the process remains simple it has several drawbacks such as high reaction temperature, larger particle size, limited degree of homogeneity, and low sinterability. On the other hand, the wet chemical processes such as sol–gel, co-precipitation, citrate-gel and combustion synthesis method yield sub-micron sized particles with good homogeneity, high sinterability, and good control of stoichiometry [14].

Further the combustion synthetic route is preferred, because of its potential advantages such as low processing time, low external energy consumption, self-sustaining instantaneous reaction, and high yield of nanosized particles. Co-precipitation method used to prepare nanocrystalline $NiFe_2O_4$ powders [15] and showed that the temperature, time and pH of reaction have been confirmed to affect the crystal size and consequently the property of nanocrystalline $NiFe_2O_4$ powders.

In the present work a series of Sn^{4+} substituted $NiFe_2O_4$ with general formula $Ni_{1+x}Fe_{2-2x}Sn_xO_4$ (x = 0.1, 0.2, 0.3, 0.4 and 0.5) has been prepared by co-precipitation synthetic method. The structural and microstructural evolution of the nanophase has been studied by X-ray powder diffraction and the Rietveld method. Several computer programs have been used for the analysis of the experimental results. The particle morphology was studied by scanning electron microscopy (SEM) and transmission electron microscopy (TEM). The different morphologies, sizes, and material properties of these spinels were analyzed and discussed.

2. Experimental

The nanocrystalline $Ni_{1+x}Fe_{2-2x}Sn_xO_4$ (x=0.0, 0.1, 0.2, 0.3, 0.4, 0.5) was prepared by co-precipitation method. Stoichiometric quantities of analytical grade $NiSo_4.6H_2o$, $FeSo_4.7H_2o$ and $Sncl_2.2H_2o$. Each starting material was weighted, all add into 100 ml de – ionized water with concentration 0.25 M, and stirred to complete dissolution. The Na OH solution is prepared by dissolving NaOH in100 ml de- ionizing water with concentration of 1 M. These two solutions mentioned above are mixed together by stirring, heated to the reaction temperature between 90 and 200 °C, a small amount of NaOH solution was continuously added to keep the pH value between 10 and 12. After the reaction, the precipitated particles are washed by de - ionizing water and filter several times then dried. After drying, the co - precipitated ferrite particles were sintered at 850 °C for x = 0 for 2h and 1000 °C for the samples of (x = 0.1, 0.2, 0.3, 0.4, 0.5) for 6h.

The structural homogeneity, crystal structure, phase formation, crystalline size were determined from XRD patterns collected using a Philips X'Pert MPP powder diffractometer with a goniometer with Cu K-Alpha radiation. The diffractometer is controlled and operated by

a PC computer which is supplied with the program PROfit, peak search and search match.

Scanning Electron Microscope (SEM) Model JEOL 6400 was used to study the micro -structure and the distribution of the size of the Sn substituted Ni nanocrystalline ferrite. Transmission electron microscopic (TEM) images were obtained on a JEOL-1230 microscope with an accelerating voltage of 100 keV.

3. Rietveld analysis of the experimental data

3.1 Structural analysis and refinement

In the Rietveld analysis, we employed the program FULLPROF Rietveld software [16, 17]. It is designed to refine simultaneously both the structural (lattice cell constants and atomic positions and occupancies) and microstructural parameters (crystallite size and r.m.s. strain). The shape of the peaks in the experimental diffraction patterns was well described by an asymmetric pseudo-Voigt (pV) function. The background of each pattern was fitted by a polynomial function of degree 5.

To simulate the theoretical X-ray powder diffraction patterns of $Ni_{1+x}Fe_{2-2x}Sn_xO_4$ the following considerations for the different phases were made:

1-Identification of the phases by Computer search-match to compare experimental pattern with ICDD database of known compounds.

2-Index the diffraction pattern to determine crystal system and unit cell dimensions and to determine space group:

(I) Iron Nickel Tin Oxide (cubic, space group: Fd-$3m$ (227), $a = 0.8395$ nm (ICDD PDF # 76-2447)) Wyckoff positions for (A) site, [B] site, and

O^{2-} are $8a$, $16d$ and $32e$, respectively.

(II) Tin Oxide (tetragonal, space group: P42 / mnm (136), a, b = 0.47382 nm, c=0.31871 nm (ICDD PDF # 72-1147).

A detailed account of the mathematical procedures implemented in the Rietveld analysis has been reported elsewhere [16–22]. In this work, we give a brief, description of the analysis of the experimental powder diffraction patterns done by us. First, the positions of the peaks were corrected for zero-shift error by successive refinements. Considering the integrated intensity of the peaks to be a function of the refined structural parameters, the Marquardt least-squares procedure was adopted for minimizing the difference between the observed and simulated powder diffraction patterns. The progress of the minimization was monitored through the usual reliability parameters, R_{wp} (weighted residual factor), and R_{exp} (expected residual factor) defined as:

$$R_{WP} = \left\{ \sum_i W_i \left[Y(obs)_i - Y(cal)_i \right]^2 \bigg/ \sum_i W_i Y(obs)_i^2 \right\}^{\frac{1}{2}} \rightarrow (1)$$

$$R_{exp} = \left[(N - P + C) \bigg/ \sum W_i Y(obs)^2 \right]^{1/2} \rightarrow (2)$$

where

Y (obs) and y (calc) the observed and calculated count rates respectively.

W_i is a suitable weight taken as: $W_i = 1/Y(obs)$ I

N is the total number of points used in the refinement

P is the number of refined parameters

C is the number of strict constraint functions

N-P+C is the number of degrees of freedom

Also, we used the so-called goodness of fit (GoF) factor [16–20]:

$$G_oF = \frac{R_{WP}}{R_{exp}} = \sqrt{\sum \frac{(Y(obs) - Y(calc))^2}{Y_{obs}} /(N - P + C)} \rightarrow \quad (3)$$

Refinements were carried out until convergence was reached and the value of the GoF factor became close to 1.

3. 2 Size-strain analysis

It has been well established that the observed broadening of the diffraction peaks is mainly due to small crystallite size and the presence of root mean square (r.m.s.) strain inside the crystallites. The crystallite size and strain broadening can be approximated with Cauchy and Gaussian type functions, respectively [19–23]. Thus, the basic consideration of the method employed in the Rietveld analysis and by us is the modeling of the diffraction profiles with an analytical function, which is a combination of Cauchy and Gauss as well as a function taking into account the asymmetry in the diffraction profile. Again, the process of successive profile refinements was adopted to refine the crystallite size and strain in the studied materials. The refinement was continued until convergence was reached and the value of the quality factor (GoF) approached 1.

4. Results and discussion

4.1 X-Ray diffraction

X-ray diffraction patterns of the co –precipitation synthesized $Ni_{1+x}Fe_{2-2x}Sn_xO_4$ (x=0.0,0.1,0.2,0.3,0.4,0.5) sintered at 850 ºC for 2 h for x = 0 and at 1000 ºC for 6 h for (x = 0.1,0.2,0.30.4,0.5) are presented in Fig. 1. The X-ray diffraction analysis by computer search matching for nanocrystalline investigated samples showed that all samples consisted of single phase spinel cubic structure and do not contain any reflection from starting, but at (x = 0.4, 0.5) x-ray diffraction analysis showed presence of two nanocrystalline phases with different lattice parameters, the predominant peaks of $Ni_{1+x}Fe_{2-2x}Sn_xO_4$ and also SnO_2 phase.
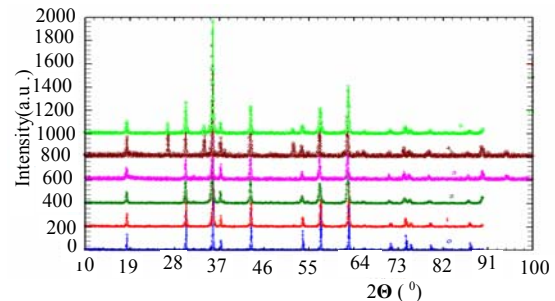

Fig. 1. X-ray diffraction pattern for $Ni_{1+x}Fe_{2-2x}Sn_xO_4$ prepared system.

The Rietveld plots of the refinements for co-precipitation prepared system are given in Fig. 2. In these figures the observed intensity data, y is plotted in the upper field as points. The calculated patterns are shown in the same field as a solid- line curve. The difference, observed minus calculated, is shown in the lower field. The short vertical bars in the middle field indicate the positions of possible Bragg reflections.
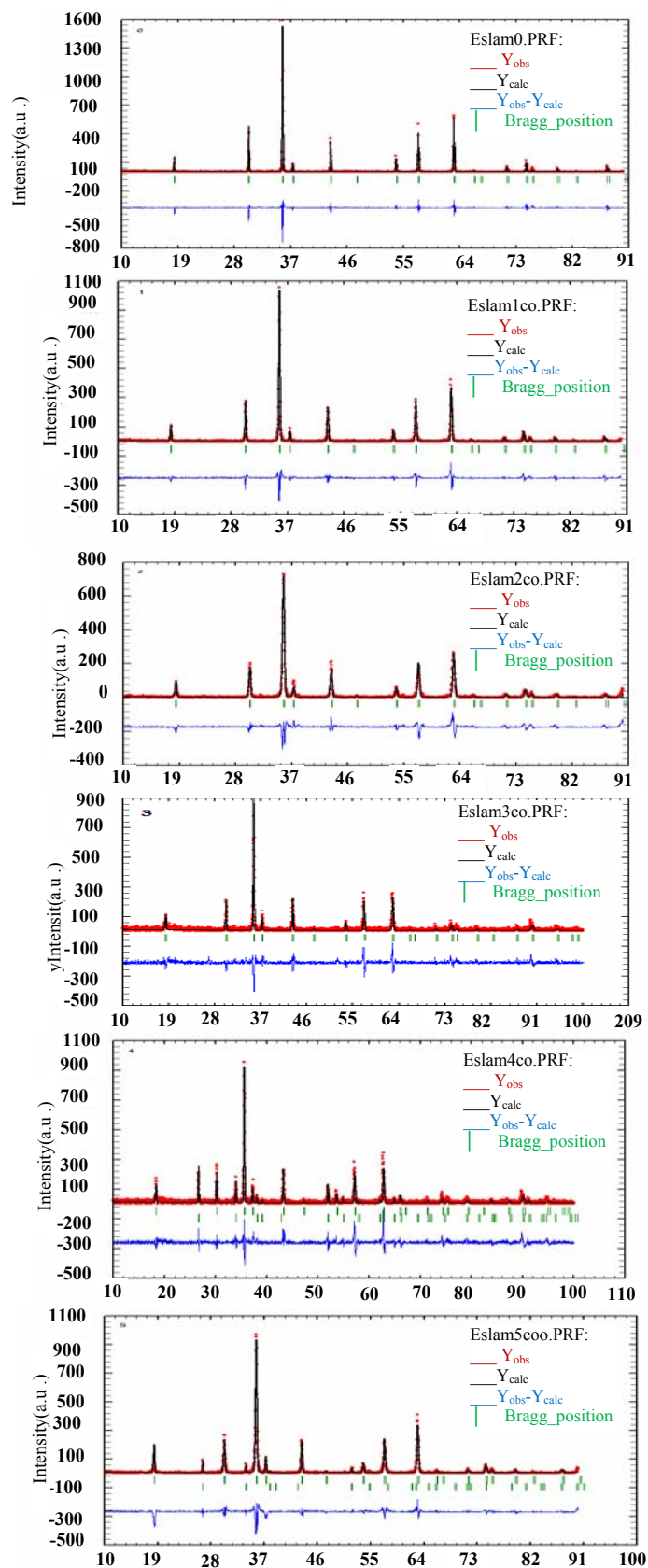
Fig. 2. The profile fitting for the prepared system.

The lattice parameter a (Å) and oxygen parameter U of the prepared system are shown in Table 1. It is evident from the table that the lattice parameter increases with increasing concentration of Sn^{4+}. This means that the lattice parameters of these spinel compounds are closely related to the size of the cations. The reason is that, the atomic radii of Sn^{4+} (0.745) is larger than Fe^{3+} (0.645) [24]. Moreover, the Sn^{4+} has a strong site preference for B site [25]. The partial replacement of Fe^{3+} by Sn^{4+} will cause the increasing of the unit cell.

Table 1. The lattice parameter a (Å) and oxygen parameter U of the prepared system.

Composition	a (Å)	U
$NiFe_2O_4$	8.335(1)	0.2549(2)
$Ni_{1.1}Fe_{1.8}Sn_{0.1}O_4$	8.337(1)	0.2549(4)
$Ni_{1.2}Fe_{1.6}Sn0.2O_4$	8.344(1)	0.2549(8)
$Ni_{1.3}Fe_{1.4}Sn0.3O_4$	8.361(1)	0.2551(7)
$Ni_{1.4}Fe_{1.2}Sn_{0.4}O_4$	8.361(7)	0.2552(8)
$Ni_{1.5}Fe Sn_{0.5}O_4$	8.364(7)	0.2553(2)

The refinement results showed that the nanocrystalline ferrite phase is partially an inverse spinel. The formation of mixed spinel instead of inverse spinel may result from that during the formation of spinel ferrite the occupancy of Fe^{3+} cation on (A) site decreases. At the same time, the occupancy of Ni^{2+} cation on [B] site decreases and then increases on (A) site. This occurs when the random distribution of cations among the (A) and [B] sites inside the spinel matrix exist. Cation distribution on A-site and B-site for the prepared system is shown in Table 2.

Table 2. Cation distribution on A-site and B-site for the prepared system.

Composition	Cation distribution (A-site)	Cation distribution (B-site)
$Ni Fe_2 O_4$	($Ni_{0.07} Fe_{0.93}$)	[$Ni_{0.93} Fe_{1.07}$]
$Ni_{1.1}Fe_{1.8}Sn_{0.1}O_4$	($Ni_{0.15} Fe_{0.85}$)	[$Ni_{0.95} Fe_{0.95} Sn_{0.1}$]
$Ni_{1.2}Fe_{1.6}Sn_{0.2}O_4$	($Ni_{0.2} Fe_{0.8}$)	[$Ni Fe_{0.8} Sn_{0.2}$]
$Ni_{1.3}Fe_{1.4}Sn_{0.3}O_4$	($Ni_{0.25} Fe_{0.75}$)	[$Ni_{1.05} Fe_{0.65} Sn_{0.3}$]
$Ni_{1.36}Fe_{1.28} Sn_{0.36}O_4$	($Ni_{0.26} Fe_{0.74}$)	[$Ni_{1.1} Fe_{0.54} Sn_{0.36}$]
$Ni_{1.43}Fe_{1.14} Sn_{0.43}O_4$	($Ni_{0.33} Fe_{0.67}$)	[$Ni_{1.1} Fe_{0.47} Sn_{0.43}$]

The X-ray diffraction analysis thus confirms site preference of Tin for octahedral coordination and Ni can also occupy A-site in addition to B-site.

The cations distribution show the strong preference of the Sn^{4+} to the octahedral site which is in very good agreement with results reported on this ion [26].

The calculated values of the inter atomic distances between the cations on the tetrahedral (A) and octahedral (B) sites for nanocrystalline $Ni_{1+x}Fe_{2-2x}Sn_xO_4$ are listed in Table 3. The shorter A –B distance is related to the fact the anion octahedral surrounding the B-site cations share edges, whereas the tetrahedral anion surrounding the A-site cations do not have any contact. Each anion in the spinel structure is surrounding by one A and three B site cations arranged in tetrahedron with the anion in the center. The angle A-O-B is 125º, and the angle B-O-B is 90^0.

Table 3. Average crystallite size calculated from Win-Fit programme.

Composition	Average crystallite size(nm)	Lattice strain
$NiFe_2O_4$	53	0.047%
$Ni_{1.1}Fe_{1.8}Sn_{0.1}O_4$	45	0.174%
$Ni_{1.2}Fe_{1.6}Sn_{0.2}O_4$	19	0.028%
$Ni_{1.3}Fe_{1.4}Sn_{0.3}O_4$	38	0.107%
$Ni_{1.4}Fe_{1.2}Sn_{0.4}O_4$	61	0.805%
$Ni_{1.5}Fe Sn_{0.5}O_4$	42	0.086%

4.2 Microstructural analysis

Rietveld analysis [16, 17, and 18] has been adopted in the present study to determine the microstructural parameters of nanocrystalline $Ni_{1+x}Fe_{2-2x}Sn_xO_4$ (x = 0.1, 0.2, 0.3, 0.4, 0.5). The analysis aims at characterizing the materials in terms of microstructural parameters such as crystallite size and root mean square (r.m.s.) lattice strain. Average crystallite size and Lattice strain calculated from Win-Fit program for the prepared samples shown in Table 3.

4.3 Scanning electron microscope (SEM)

The microstructure and surface morphology was observed with a scanning electron microscopy (SEM). SEM representative micrographs for the nanocrystalline $Ni_{1+x}Fe_{2-2x}Sn_xO_4$ ferrite system prepared by co-precipitation method shown in Fig. 3 .The surface morphology of all the samples as seen from the SEM consists of well-crystallized grains, with relatively homogeneous grain distribution, The average grain size varying from 1 to 3μm.
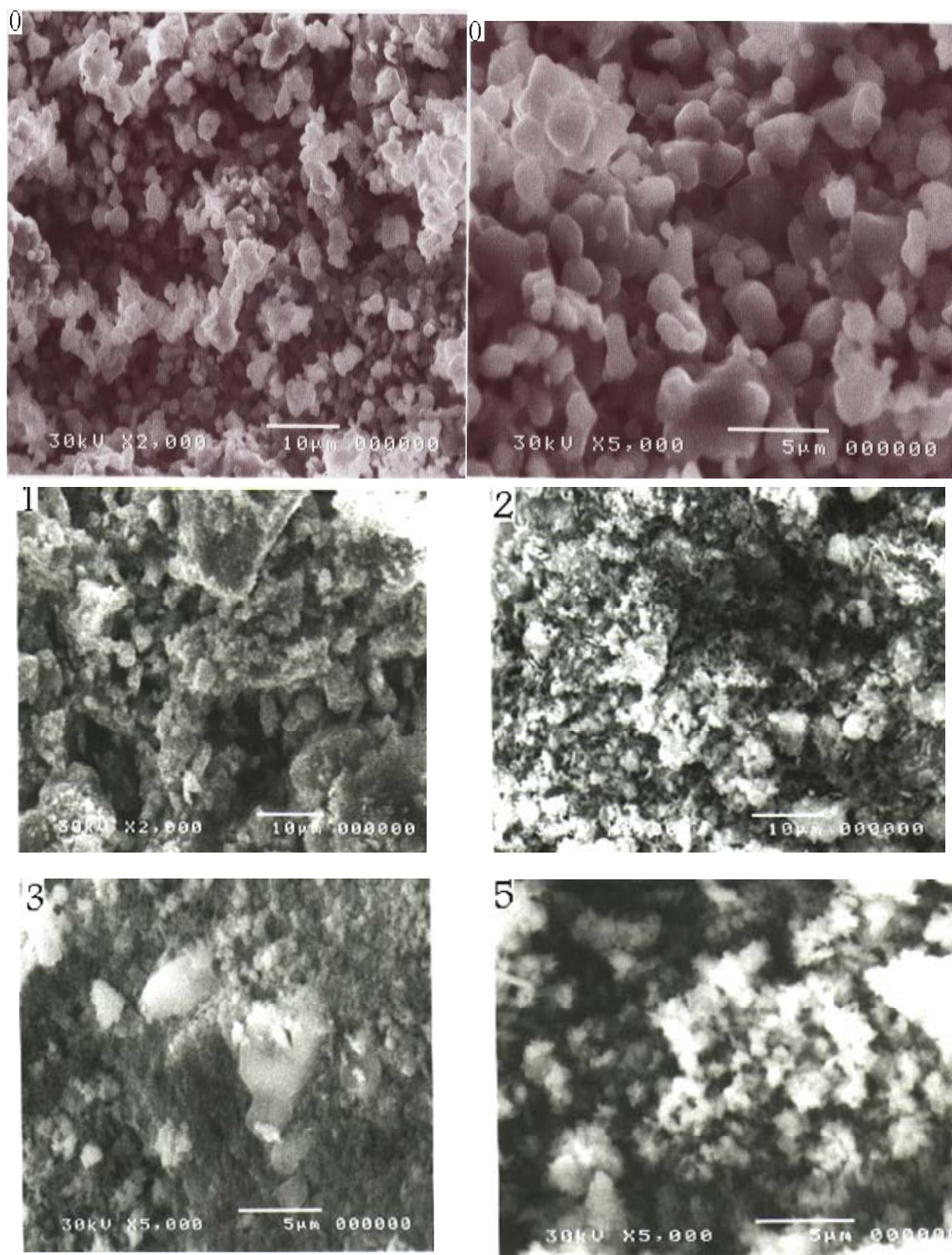
Fig. 3. SEM for the $Ni_{1+x}Fe_{2-2x}Sn_xO_4$ prepared system where 0, 1, 2, 3, 5 refer respectively to x=0.0, 0.1, 0.2, 0.3, 0.5.

4.4 Transmission electron microscope (TEM)

TEM micrograph reveals that the grains of sample are spherical in shape and average size of the grain varying from 20 to 70 nm which is quite closer to the X-ray crystallite size. The shape of the precipitated particles becomes regular and the distribution of particle size is uniform. However, some of the particles are quite larger due to agglomeration of small grains and variation in density of grains. TEM micrograph for Ni Fe_2O_4 and $Ni_{1.1}$ $Fe_{1.8}Sn_{0.1}O_4$ samples shown in Fig. 4.
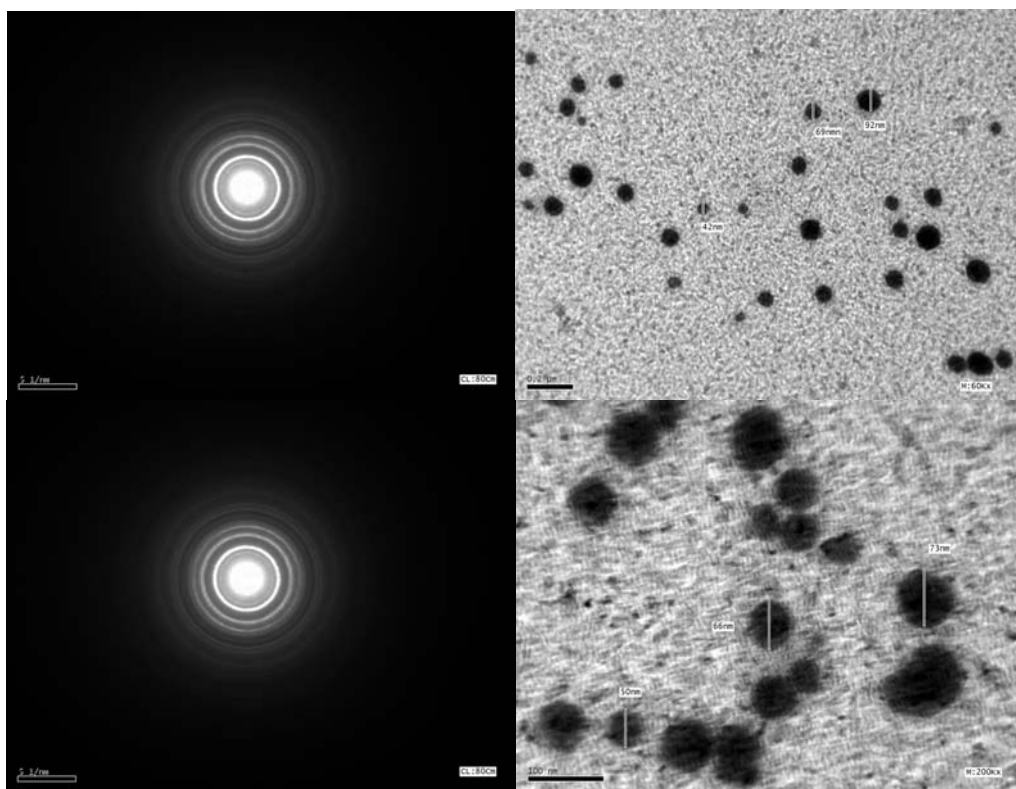
Fig. 4. Transmission electron microscope (TEM) for Ni Fe_2O_4 and $Ni_{1.1}$ $Fe_{1.8}Sn_{0.1}O_4$ prepared samples.

5. Conclusions

The wet chemical co-precipitation has been successfully used for the preparation of mixed spinel ferrites with nanosize particles; provide the higher degree of homogenization of reactant and, lower temperatures are sufficient for the reaction to occur, high sinterability, and good control of stoichiometry. It has been also experimentally verified that the distribution of cations among the lattice sites depends on material's preparation.

The refinement results showed that the nanocrystalline ferrite phase is partially an inverse spinel. The formation of mixed spinel instead of inverse spinel may result from that during the formation of spinel ferrite the occupancy of Fe^{3+} cation on (A) site decreases. At the same time, the occupancy of Ni^{2+} cation on [B] site decreases and then increases on (A) site.

The surface morphology of all the samples as seen from the SEM consists of well-crystallized grains, with relatively homogeneous grain distribution, with an average grain size varying from 1 to 3 μm.

TEM micrograph reveals that the grains of sample are spherical in shape and average size of the particles is between (20-70) nm which is quite closer to the X-ray crystallite size.

References

[1] L. Sathyanarayana, K. Madusudhan Reddy, S. V. Manorama, Mater.Chem. Phys. **82**, 21 (2003).
[2] R. Alcantra, M. Jaraba, P. Lavela, J. L. Tirado, J. C. Jumas, J. Oliver,Electrochem. Commun. **5**, 16 (2003).
[3] Q. Yitai, X. Yi, L. Jing, C. Zuyao, Y. Li, Mater. Sci. Eng. B **34**, 11 (1995).
[4] V. K. Sankaranarayanan, C. SreeKumar, Curr. Appl. Phys. **3**, 205 (2003).
[5] P. Yadoji, R. Peelamedu, D. Agrawal, R. Roy, Mater. Sci. Eng. B**98**, 269 (2003).
[6] B. K. Labde, M. C. Cable, N. R. Sham Kumar, Mater. Lett. **57**, 1651 (2003).
[7] Z. Yue, L. Li, J. Zhou, H. Zhang, Z. Gui, Mater. Sci. Eng. B **64**, 68 (1999).
[8] D. Ravinder, S. Srinivasa Rao, P. Shalini, Mater. Lett. **57**, 4040 (2003).
[9] Giang-Min. Kui, Jian-bao, Y. C. Han, Mater. Chem. Phys. **74**, 340 (2002).
[10] M. Z. Said, Mater. Lett. **34**, 305 (1998).
[11] L. John Berchmans, R. Kalai Selvan, P. N. Selva Kumar, C. O. Augustin, J. Magn. Magn. Mater. **279**, 103 (2004).
[12] D.-C. Boe, S. woo Kim, H.-W. Lee, K. S. Han, Mater. Lett. **57**, 1997 (2003).

[13] J. S. Baijal, D. Kothari, S. P. C. Prakash, Solid State Commun. **69**, 277 (1989).

[14] D. Siegel, J. Mater. Chem. **7**, 1297 (1999).

[15] M. M. Rashad, O. A. Fouad, Materials Chemistry and Physics **94,** 365 (2005).

[16] H. M. Rietveld, Acta Crystallography **22,** 151 (1967).

[17] H. M. Rietveld, J. Appl. Crystallogr. **2**, 65 (1969).

[18] L. Lutterotti, MAUDWEB, Version 1.9992, 2004. http://www.ing.unitn.it/<luttero/maud.

[19] S. Bid, S. K. Pradhan, J. Appl. Crystallogr. **35**, 517 (2002).

[20] S. Bid, S. K. Pradhan, Mater. Chem. Phys. **82**, 27 (2003).

[21] H. Dutta, S. K. Manik, S. K. Pradhan, J. Appl. Crystallogr. **36**, (2003) 260.

[22] S. K. Manik, S. K. Pradhan, Mater. Chem. Phys. **86**, 284 (2004).

[23] J. G. M. Van Berkum, Ph. D. Thesis, Delft University of Technology,The Netherlands, 1994.

[24] S. C. O'Neill, A. Navrotsky, Am. Mineral. **68**, 181 (1983).

[25] S. V. Kakatkar, Ph. D. Thesis, Shivaji University, Kolhapur, India, 1993.

[26] P. M. Lamber, P. P. Edwards, M. R. Harrison, J. Solid State. Chem. **9**, 345 (1990).

_____
[*]Corresponding author: zeinab_ali56@yahoo.com